International Scientific Conference 20 UNITECH 26

INTERNATIONAL SCIENTIFIC CONFERENCE
19-21 November 2026
GABROVO

NUMERICAL INVESTIGATION OF THE EFFECT OF CHANNEL INTERIOR ANGLE ON HEAT TRANSFER AND PUMPING POWER IN ZIGZAG MICROCHANNELS

Damla Özgür

Trakya University, Edirne, Turkey

……

damlaadli@trakya.edu.tr

Abstract

This study numerically examines the effects of channel interior angle on heat transfer and hydraulic pumping power in zigzag microchannels. A channel comprising seven straight segments is considered, with interior angles of 135°, 150°, and 165°, where 180° denotes a straight channel. Steady-state, laminar conjugate heat transfer in a water–aluminum system is evaluated at an inlet temperature of 292 K, inlet velocities of 0.1–0.8 m/s, and bottom-wall temperatures of 330–360 K. The heat transfer rate, reference heat transfer coefficient, reference Nusselt number, and pressure drop are compared. At an inlet velocity of 0.8 m/s and a bottom-wall temperature of 360 K, decreasing the interior angle from 165° to 135° increases the heat transfer rate by approximately 18.79%, the reference Nusselt number by 34.00%, and the hydraulic pumping power by 58.91% at the same volumetric flow rate. The findings indicate that a smaller interior angle enhances cooling capacity but requires greater pumping power. Accordingly, channel angle selection should account for both thermal enhancement and hydraulic requirements, together with the associated changes in channel length and heat transfer surface area.

Keywords: Zigzag microchannel, channel interior angle, conjugate heat transfer, pressure drop, pumping power.

1. INTRODUCTION

Removing concentrated heat loads from electronic components requires compact cooling systems with sufficient thermal capacity and acceptable pumping power. Microchannel performance depends on fluid flow, convection, and heat conduction through the solid substrate. Geometric modifications must therefore be assessed in terms of both heat removal and hydraulic demand.

Mohammed et al. [1] compared microchannel shapes using three-dimensional conjugate heat transfer simulations. Among the investigated configurations, the zigzag channel provided the highest heat transfer coefficient, pressure drop, and friction factor. Dai et al. [2] experimentally studied water flow in zigzag and sinusoidal microchannels and reported enhanced heat transfer with increased pressure loss relative to an equivalent straight channel. Gaikwad and Nalawade [3] experimentally compared straight and zigzag channels with different wavelengths and amplitudes, observing the same thermal–hydraulic trade-off. Peng et al. [4] experimentally investigated a zigzag-serpentine heat sink with deionized water at incidence angles of 30°, 45°, 60°, and 90°. The lowest pressure drops and thermal resistance occurred at 30°, whereas 45° provided the most uniform surface temperature. Their incidence angle differs from the interior-angle definition used here. Using thermal resistance and pressure drop as performance measures, they found hydraulic diameter more influential than orientation angle within the studied range. Staszak and Musielak [5] investigated conjugate heat transfer in zigzag microchannels with different segment counts, inlet velocities, and heated-bottom temperatures, providing the physical and operational reference for the present study.

This is an open access article licensed under Creative Commons Attribution 4.0 International
Print ISSN: 1313-230X, Online ISSN: 3033-1404

For wavy microchannels, Sui et al. [6] reported secondary flows that promoted mixing and heat transfer. Lin et al. [7] varied wavelength and amplitude along the flow direction and evaluated thermal resistance and bottom-temperature nonuniformity at constant pumping power. Their proposed configurations improved performance under this constraint. Petkov et al. [8] and Petkov and Zimparov [9] evaluated fully developed laminar flow in non-circular ducts under H1 conditions, using circular tubes as the reference at equal flow cross-sectional area. Performance benefits depended on design objectives and constraints. For tube inserts, Zimparov et al. [10] emphasized the effects of surface area, mass flow rate, inlet temperature, and external thermal resistance on performance comparisons. These findings support consistent comparison constraints in the present zigzag-channel analysis.

These studies show that flow-path geometry and comparison constraints jointly determine the assessed thermal benefit. At a fixed axial length, changing the zigzag interior angle also changes the actual flow-path length and solid–fluid contact area. Heat transfer differences must therefore be interpreted with these geometric effects in addition to flow redistribution and mixing.

The present study considers seven-segment water–aluminum microchannels with interior angles of 135°, 150°, and 165°, corresponding to flow deflections of 45°, 30°, and 15°. Steady laminar conjugate heat transfer is evaluated at a 292 K inlet temperature, velocities of 0.1–0.8 m/s, and bottom temperatures of 330–360 K. The contribution is a joint assessment of heat transfer rate, reference heat transfer coefficient, reference Nusselt number, pressure drop, and hydraulic pumping power over 96 conditions, accounting for angle-dependent changes in channel length and surface area.

In this study, the thermal–hydraulic performance of seven-segment water–aluminum zigzag microchannels with interior angles of 135°, 150°, and 165° is investigated. The contribution lies in jointly evaluating heat transfer enhancement and pumping requirements while accounting for angle-dependent changes in channel length and interface area. This assessment is important because increased cooling capacity alone does not establish the suitability of channel geometry. The findings provide a consistent basis for comparing geometric alternatives and balancing heat removal against hydraulic demand in compact cooling systems.

2. ANALYSIS

This study aimed to investigate the forced-convection cooling performance of water in a zigzag microchannel formed within an aluminum body. The bottom of the solid body was defined as a heated surface maintained at a constant temperature, and the fluid was assumed to enter the channel at a specified velocity and temperature. A three-dimensional conjugate heat transfer model was formulated by considering heat conduction in the solid region together with convection and conduction in the fluid region.

The channel geometry was defined as seven straight segments connected by six internal turns. The channel interior angle, β, was defined using the geometric convention in which a straight channel corresponds to 180°. The relationship between the flow deflection angle, θ, and the channel interior angle was expressed as:

$$\theta = 180^\circ - \beta \qquad (1)$$

Interior angles of 135°, 150°, and 165° corresponded to flow deflections of 45°, 30°, and 15°, respectively. With successive segments inclined symmetrically about the main axis, the segment inclination was:

$$\alpha = \frac{\theta}{2} \qquad (2)$$

For a projected axial length of $L_z = 80$ mm, the actual centerline length was calculated as:

$$L_c = \frac{L_z}{\cos\alpha} \quad (3)$$

Interior angles of 165°, 150°, and 135° yielded centerline lengths of approximately 80.69, 82.82, and 86.59mm, respectively. The resulting changes in channel length and solid–fluid contact area were included in the interpretation of thermal performance.

The cross section followed Staszak and Musielak [5]. In the symmetry-reduced domain, fluid width, fluid height, solid-body width, and total height were 1mm, 0.5mm, 3mm, and 1mm, respectively. Reflection across the symmetry plane gave a physical fluid cross section of $1 \times 1\text{mm}^2$ and the hydraulic diameter:

$$D_h = \frac{4A_c}{P_w} = 1\text{mm} \quad (4)$$

Here, A_c is the physical flow area and P_w the wetted perimeter. The symmetry surface was excluded from the wetted perimeter because it is not a physical wall.

The flow was assumed to be steady, three-dimensional, laminar, and single-phase. Water was treated as Newtonian, with temperature-dependent density and viscosity. Pressure-dependent properties, gravity, radiation, viscous dissipation, internal heat generation, and interfacial thermal contact resistance were neglected.

The inlet temperature was 292K. The proposed operating range comprised inlet velocities of 0.1–$0.8\text{m}/s$ and bottom temperatures of 330, 340, 350, and 360K. Water properties were specified as:

$$c_p = 4182\text{J kg}^{-1}\text{K}^{-1}, k_f = 0.6\text{W m}^{-1}\text{K}^{-1} \quad (5)$$

The aluminum thermal conductivity was:

$$k_s = 202.4\text{W m}^{-1}\text{K}^{-1} \quad (6)$$

Density and viscosity were to be evaluated using the temperature correlations in [6].

Steady mass conservation was written as:

$$\nabla \cdot (\rho \mathbf{u}) = 0 \quad (7)$$

The conservative form accounts for temperature-dependent density; no additional zero-divergence velocity constraint was imposed.

Momentum conservation was expressed as:

$$\nabla \cdot (\rho \mathbf{u} \otimes \mathbf{u}) = -\nabla p + \nabla \cdot \boldsymbol{\tau} \quad (8)$$

Under Stokes' hypothesis, the Newtonian viscous stress tensor was:

$$\boldsymbol{\tau} = \mu \left[\nabla \mathbf{u} + (\nabla \mathbf{u})^T - \frac{2}{3}(\nabla \cdot \mathbf{u})\mathbf{I} \right] \quad (9)$$

The stress-tensor formulation retained spatial viscosity variations. The fluid energy equation was:

$$\nabla \cdot \left(\rho c_p \mathbf{u} T_f \right) = \nabla \cdot \left(k_f \nabla T_f \right) \quad (10)$$

For constant specific heat and satisfied mass conservation, this reduced to:

$$\rho c_p \mathbf{u} \cdot \nabla T_f = \nabla \cdot \left(k_f \nabla T_f \right) \quad (11)$$

Steady conduction in the solid was governed by:

$$\nabla \cdot (k_s \nabla T_s) = 0 \quad (12)$$

Constant solid thermal conductivity gives the Laplace equation. Uniform inlet conditions were prescribed as:

$$\mathbf{u} = U_{\text{in}} \mathbf{e}_{\text{in}}, \qquad T_f = T_{\text{in}}. \quad (13)$$

Here, $\mathbf{e}_{\text{in}}$ points from the inlet into the computational domain. No independent pressure condition was imposed at this velocity inlet. The outlet gauge pressure was:

$$p_{\text{out}} = 0. \quad (14)$$

For outflow without backflow, zero normal gradients were imposed:

$$\frac{\partial \mathbf{u}}{\partial n} = 0, \qquad \frac{\partial T_f}{\partial n} = 0 \quad (15)$$

No slip was prescribed at the solid–fluid interface:

$$\mathbf{u} = \mathbf{0} \tag{16}$$

Interfacial temperature continuity required:

$$T_s = T_f \tag{17}$$

Using the same normal direction on both sides, interfacial heat-flux continuity required:

$$k_s \frac{\partial T_s}{\partial n} = k_f \frac{\partial T_f}{\partial n} \tag{18}$$

The solid bottom was maintained at:

$$T_s = T_{\text{base}} \tag{19}$$

The remaining adiabatic external surfaces satisfied:

$$-k_s \nabla T_s \cdot \mathbf{n} = 0. \tag{20}$$

At the symmetry plane, normal velocity and the normal gradients of tangential velocity, temperature, and pressure were zero. This condition differs from the no-slip condition at physical walls.

A cell-centered finite volume method was proposed for MATLAB implementation. Conservation equations were integrated over each control volume using shared face fluxes between adjacent cells. The discrete general transport equation was:

$$\sum_f F_f \, \phi_f = \sum_f \Gamma_{\phi,f} \, (\nabla \phi)_f \cdot \mathbf{S}_f + S_{\phi,P} V_P \tag{21}$$

The face mass flow rate was:

$$F_f = \rho_f \mathbf{u}_f \cdot \mathbf{S}_f \tag{22}$$

Interfacial thermal conductance accounted for the cell-center distances to the interface and the respective conductivities:

$$G_f = \frac{A_f}{\delta_f / k_f + \delta_s / k_s} \tag{23}$$

The interfacial heat transfer rate was:

$$\dot{Q}_f = G_f \left(T_s - T_f \right) \tag{24}$$

Pressure and velocity were decomposed as:

$$p = p^* + p', \qquad \mathbf{u} = \mathbf{u}^* + \mathbf{u}' \tag{25}$$

Pressure corrections were to be obtained from continuity and used to update cell velocities and face mass flow rates together. Sequential linearization was proposed, with density and viscosity updated at each outer iteration. Momentum-weighted face-velocity interpolation was proposed to suppress spurious pressure oscillations on the collocated grid. The resulting sparse systems were:

$$\mathbf{A}_{\boldsymbol{\phi}} \boldsymbol{\phi} = \mathbf{b}_{\boldsymbol{\phi}} \tag{26}$$

Convergence was to be assessed from solver residuals, mass and energy balances, and successive changes in pressure drop, outlet temperature, and total heat transfer rate. The relative mass imbalance was:

$$\varepsilon_m = \frac{|\dot{m}_{\text{in}} - \dot{m}_{\text{out}}|}{\dot{m}_{\text{in}}} \tag{27}$$

Pressure drop was defined using area-averaged inlet and outlet static pressures:

$$\Delta p = \overline{p}_{\text{in}} - \overline{p}_{\text{out}}. \tag{28}$$

The outlet temperature was defined by the mass-flow-weighted average:

$$T_{\text{out}} = \frac{\int_{A_{out}} \rho u_n T \, dA}{\int_{A_{out}} \rho u_n \, dA} \tag{29}$$

The sensible heat gain of the fluid was:

$$\dot{Q}_{\text{fluid}} = \dot{m} c_p (T_{\text{out}} - T_{\text{in}}) \tag{30}$$

Axial conduction was to be included when comparing this quantity with the total interfacial heat transfer rate.

Hydraulic pumping power was based on the inlet volumetric flow rate:

$$P_h = \Delta p \, \dot{V}_{\text{in}} \tag{31}$$

Electrical power consumption requires pump and motor efficiency.

For comparison with the reference study, the heat transfer coefficient and Nusselt number were defined as:

$$h_{\mathrm{ref}} = \frac{\dot{Q}}{A_{\mathrm{ref}}(\overline{T}_{sf} - \overline{T}_f)}, \quad Nu_{\mathrm{ref}} = \frac{h_{\mathrm{ref}} D_h}{k_f} \qquad (32)$$

Here, $\overline{T}_{sf}$ and $\overline{T}_f$ are the area-averaged interface and volume-averaged fluid temperatures. This reference coefficient differs from one based on local bulk temperature and actual heat transfer area. Consistent area and temperature definitions were therefore required when comparing geometries and literature results.

3. CONCLUSION

The results were evaluated to establish how channel interior angle, inlet velocity, and bottom temperature jointly affect heat removal and hydraulic demand. The comparison covers 96 operating conditions for $\beta = 135°, 150°, 165°$, eight inlet velocities from 0.1 to 0.8 m/s, and four bottom temperatures from 330 to 360K, with $T_{\mathrm{in}} = 292$ K. The interior angle is related to the flow deflection angle by $\theta = 180° - \beta$. All heat transfer rates and hydraulic powers reported below refer to the symmetry-reduced half-channel domain. Figures 1–5 were prepared from the associated numerical tables for the 504,000-cell mesh. Percentage changes were calculated from the unrounded values; angle comparisons use $\beta = 165°$ as the reference.

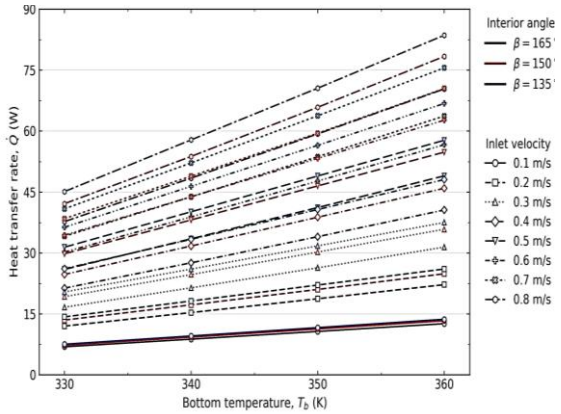


Fig.1. *Heat transfer rate versus bottom temperature for different interior angles and inlet velocities.*

Figure 1 compares $\dot{Q}$ as a function of T_{b} for the three interior angles and eight inlet velocities. Heat removal increased with both velocity and bottom temperature, while smaller interior angles produced higher values at the same operating conditions. At $U_{\mathrm{in}} = 0.8\ \mathrm{m\ s^{-1}}$ and $T_{\mathrm{b}} = 360$ K, $\dot{Q}$ increased from 70.39 W at $\beta = 165°$ to 78.40 W at $\beta = 150°$ and 83.61 W at $\beta = 135°$. The reduction from 165° to 135° therefore yielded an increase of 18.79%. At 0.8 m/s, raising the bottom temperature from 330 to 360 K increased $\dot{Q}$ by 86.56%, 86.06%, and 85.32% for interior angles of 165°, 150°, and 135°, respectively. This strong temperature dependence primarily reflects the increased thermal driving force. The angle dependence includes both the response of the flow and temperature fields and the increase in actual channel length and heat transfer area.

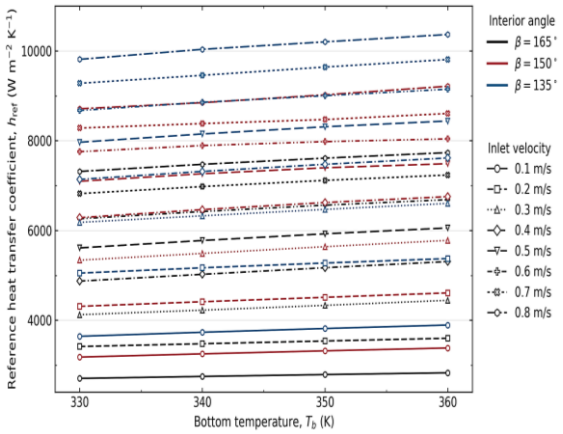


Fig.2. *Reference heat transfer coefficient versus bottom temperature for different interior angles and inlet velocities.*

Figure 2 shows the variation of h_{ref} with bottom temperature and inlet velocity. At $U_{\mathrm{in}} = 0.8\ \mathrm{m/s}$ and $T_{\mathrm{b}} = 360$ K, the reference coefficients were 7737.78, 9216.30, and 10368.62 $\mathrm{W\,m^{-2}\,K^{-1}}$ for interior angles of 165°, 150°, and 135°, respectively. The smallest interior angle thus provided a 34.00% increase relative to 165°. By comparison, increasing the bottom temperature from 330 to 360 K at the same velocity increased h_{ref} by only 5.65–5.77%. The much larger corresponding increase in $\dot{Q}$ in Figure 1 therefore cannot be attributed solely to a higher heat transfer coefficient.

Because h_{ref} is defined using a fixed reference area and averaged interface and fluid temperatures, it represents a comparative performance measure rather than a local convection coefficient. Its angle dependence should consequently be interpreted together with changes in actual surface area.

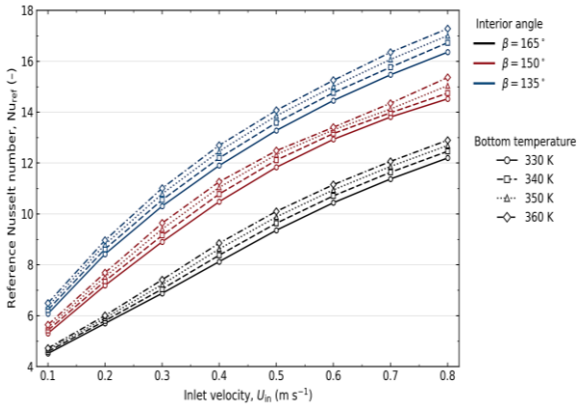


Fig.3. *Reference Nusselt number versus inlet velocity for different interior angles and bottom temperatures.*

Figure 3 compares $\mathrm{Nu_{ref}}$ over the inlet-velocity range at the four bottom temperatures. At 360 K, increasing the velocity from 0.1 to 0.8 m/s raised $\mathrm{Nu_{ref}}$ from 4.721 to 12.896, from 5.642 to 15.361, and from 6.494 to 17.281 for interior angles of 165°, 150°, and 135°, respectively. These changes correspond to increases of 173.15%, 172.25%, and 166.10%. Since $\mathrm{Nu_{ref}} = \frac{h_{\mathrm{ref}} D_{\mathrm{h}}}{k_{\mathrm{f}}}$ and both D_{h} and k_{f} are fixed, the percentage changes in $\mathrm{Nu_{ref}}$ and h_{ref} are identical. The higher values at smaller interior angles consistent with flow redirection and thermal boundary-layer redevelopment, although the integral results alone do not establish the detailed vortex structure. The simultaneous influence of velocity and geometry is therefore evident, whereas the temperature effect is comparatively modest.

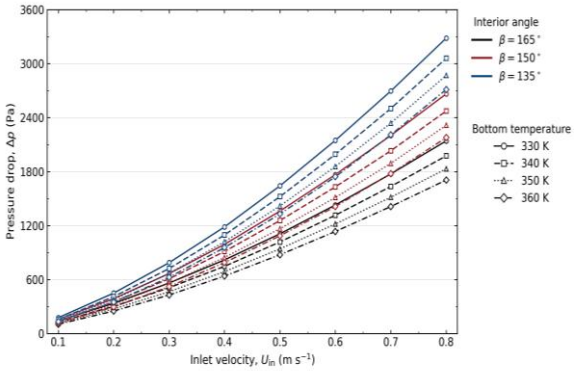


Fig.4. *Pressure drops versus inlet velocity for different interior angles and bottom temperatures.*

Figure 4 compares the pressure drop across the investigated channels. Pressure drops increased nonlinearly with inlet velocity and were highest at the smallest interior angle. At $U_{\mathrm{in}} = 0.8\ \mathrm{m/s}$ and $T_{\mathrm{b}} = 360\ \mathrm{K}$, Δp was 1708.33, 2178.97, and 2714.69 Pa for interior angles of 165°, 150°, and 135°, respectively. The corresponding hydraulic powers, calculated from $P_{\mathrm{h}} = \Delta \mathrm{p} \dot{V}_{\mathrm{in}}$ using $A_{\mathrm{in}} = 5 \times 10^{-7}\ \mathrm{m}^2$, were 0.683, 0.872, and 1.086 mW. At the same volumetric flow rate, reducing the interior angle from 165° to 135° increased both pressure drop and hydraulic pumping power by 58.91%. This penalty exceeded the 18.79% heat-transfer gain, causing $\frac{\dot{Q}}{P_{\mathrm{h}}}$ to decrease by25.25%. Conversely, increasing the bottom temperature from 330 to 360 K at 0.8 m/s reduced the pressure drop by 20.29%, 18.27%, and 17.37%, respectively, consistent with reduced viscous resistance as the water temperature increased. These powers describe hydraulic work; electrical consumption additionally depends on pump and motor efficiency.

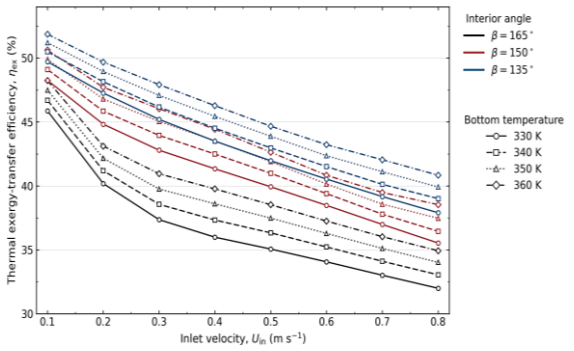


Fig.5. *Mixed-outlet thermal exergy-transfer efficiency versus inlet velocity for different interior angles and bottom temperatures.*

Figure 5 presents the mixed-outlet thermal exergy-transfer efficiency, defined as:

$$\eta_{\mathrm{ex}} = \frac{\Delta \dot{E}_{\mathrm{water}}}{\dot{Q}_{\mathrm{b}}\left(1 - \frac{T_0}{T_{\mathrm{b}}}\right) + P_{\mathrm{h}}}$$

Here, $\dot{Q}_{\mathrm{b}}$ denotes the heat supplied through the bottom, $\Delta \dot{E}_{\mathrm{water}}$ is the coolant's thermal exergy increase, and $T_0 = T_{\mathrm{in}} = 292$ K. At 360 K, increasing the inlet velocity from 0.1 to 0.8 m/s reduced η_{ex} from 48.24% to 34.94%, from 50.63% to 38.54%, and from 51.87% to 40.84% for interior angles of 165°, 150°, and 135°, respectively. The decreases were 13.30, 12.09, and 11.03 percentage points. At 0.8 m/s and 360 K, the smallest interior angle exceeded the 165° case by 5.91 percentage points. The reduction with velocity occurred despite greater heat removal: for $\beta = 135°$, the outlet temperature decreased from 357.70 to 342.15 K, reducing the thermal exergy gained per unit heat transferred. This metric describes thermal exergy transfer to the coolant and should not be interpreted as electrical efficiency or as a standalone criterion for cooling performance.

In this study, reducing the channel interior angle from 165° to 135° enhanced heat removal but increased hydraulic demand. At 0.8 m/s and 360 K, the increases in $\dot{Q}$, $\mathrm{Nu}_{\mathrm{ref}}$, and P_{h} were 18.79%, 34.00%, and 58.91%, respectively. The 135° channel therefore provided the greatest heat removal at the same inlet velocity, whereas the 165° channel required less pumping power. The approximately 7.31% increase in actual channel length and interface area also contributes to the comparison. An optimum angle cannot be established without a specified thermal duty or an equal-pumping-power comparison. The available single-mesh results further require systematic grid-refinement and discretization-sensitivity assessments before discretization uncertainty can be quantified.

REFERENCES

[1] Mohammed, H. A., Gunnasegaran, P., & Shuaib, N. H. (2011). Influence of channel shape on the thermal and hydraulic performance of microchannel heat sink. International Communications in Heat and Mass Transfer, 38(4), 474–480.

[2] Dai, Z., Fletcher, D. F., & Haynes, B. S. (2015). Impact of tortuous geometry on laminar flow heat transfer in microchannels. International Journal of Heat and Mass Transfer, 83, 382–398.

[3] Gaikwad, S. M., & Nalawade, M. K. (2022). Investigation of heat transfer and fluid flow characteristics in straight and zigzag microchannels with water as working medium. International Journal of Ambient Energy, 43(1), 5006–5012.

[4] Peng, Y., Li, Z., Li, S., Cao, B., Wu, X., & Zhao, X. (2021). The experimental study of the heat ransfer performance of a zigzag-serpentine microchannel heat sink. International Journal of Thermal Sciences, 163, Article 106831.

[5] Staszak, M., & Musielak, G. (2024). Numerical simulations of flow and heat exchange in zigzag-shaped microchannels. Applied Sciences, 14(21), Article 9826.

[6] Sui, Y., Teo, C. J., Lee, P. S., Chew, Y. T., & Shu, C. (2010). Fluid flow and heat transfer in wavy microchannels. International Journal of Heat and Mass Transfer, 53(13–14), 2760–2772.

[7] Lin, L., Zhao, J., Lu, G., Wang, X. D., & Yan, W. M. (2017). Heat transfer enhancement in microchannel heat sink by wavy channel with changing wavelength/amplitude. International Journal of Thermal Sciences, 118, 423–434.

[8] Petkov, V. M., Zimparov, V. D., & Bergles, A. E. (2013). Performance evaluation of laminar fully developed flow through ducts with non-circular shapes subjected to H1

boundary condition. Part 1. International Review of Chemical Engineering, 5(1), 1–15.
[9] Petkov, V. M., & Zimparov, V. D. (2013). Performance evaluation of laminar fully developed flow through ducts with non-circular shapes subjected to H1 boundary condition. Part 2. International Review of Chemical Engineering, 5(2), 74–87.
[10] Zimparov, V. D., Penchev, P. J., & Bonev, P. J. (2025). Heat transfer enhancement with tube inserts: How can we define the best benefit? Thermal Science, 29(1 Part B), 509–520.